*Brain Cell Biology* Volume 35, 57–73, 2006
DOI: 10.1007/s11068-006-9007-7

# Calcium-induced exocytosis from actomyosin-driven, motile varicosities formed by dynamic clusters of organelles

**Guy Malkinson[#], Zohar M. Fridman[#], Dotan Kamber, Ada Dormann, Eli Shapira and Micha E. Spira***
Department of Neurobiology, Institute of Life Sciences, The Hebrew University of Jerusalem, Jerusalem 91904, Israel (*author for correspondence; e-mail: spira@cc.huji.ac.il)
[#]These authors contributed equally to the paper.

Received 13 August 2006; Revised 2 November 2006; Accepted 22 November 2006
Published online 10 March 2007

**Varicosities are ubiquitous neuronal structures that appear as local swellings along neurites of invertebrate and vertebrate neurons. Surprisingly little is known about their cell biology. We use here cultured *Aplysia* neurons and demonstrate that varicosities are motile compartments that contain large clusters of organelles. The content of varicosities propagate along neurites within the plasma membrane "sleeve", split and merge, or wobble in place. Confocal imaging, retrospective immunolabeling, electron microscopy and pharmacological perturbations reveal that the motility of the varicosities' organelle content occurs in concert with an actin scaffold and is generated by actomyosin motors. Despite the motility of these organelle clusters within the cytoplasm along the neurites, elevation of the free intracellular calcium concentration within varicosities by trains of action potentials induces exocytosis followed by membrane retrieval. Our observations demonstrate that varicosities formed in the absence of postsynaptic cells behave as "ready to go" prefabricated presynaptic terminals. We suggest that the varicosities' motility serves to increase the probability of encountering a postsynaptic cell and to rapidly form a functional synapse.**

## Introduction

Varicosities (VRs) are ubiquitous neuronal structures that appear as local swellings along neurites of invertebrates and vertebrates, for example, *Helix* neurons (Cibelli et al., 1996; Fiumara et al., 2001); *Aplysia* neurons (Hatada et al., 2000; Grabham et al., 2005); fish retinal explants (Koenig et al., 1985); rat cortical neurons (Morgenthaler et al., 2003); rat granule cells (Urakubo et al., 2003); pyramidal neurons (Umeda et al., 2005); and hippocampal neurons (Krueger et al., 2003; Sankaranarayanan et al., 2003). In culture, VRs can be formed by neurons that have not made contact with postsynaptic cells, as well as by neurons that form *en passant* synapses where they are often referred to as presynaptic boutons (Hatada et al., 1999). VRs are formed *de novo* in neurons grown in isolation, either at the tips of advancing growth cones (GCs), or along neurites after the GCs have advanced, or by splitting of preexisting VRs (Hatada et al., 1999, 2000; Grabham et al., 2005).

Electron microscope studies revealed that the content of VRs formed by neurons grown in the absence of postsynaptic targets ranges from VRs containing high densities of organelles to VRs that are almost free of organelles (Koenig et al., 1985;

**Electronic Supplementary Material** Supplementary material is available in the online version of this article at http://dx.doi.org/10.1007/s11068-006-9007-7

Shepherd and Harris, 1998). VRs formed by cultured goldfish retinal ganglion cells exhibited bulk anterograde and retrograde vectorial movements at a mean velocity of 0.218 $\pm$ 0.068 $\mu$m/s (Koenig et al., 1985). Slow translocation rates of presynaptic VRs in contact with dendritic spines of hippocampal neurons were also recently reported (Umeda et al., 2005).

A number of reports demonstrate that VRs, neuronal shafts and GCs can be induced to exocytose by potassium depolarization before the establishment of contact with postsynaptic elements (Sun and Poo, 1987; Matteoli et al., 1992; Kraszewski et al., 1995; Dai and Peng, 1996; Marxen et al., 1999; Zakharenko et al., 1999; Krueger et al., 2003; Morgenthaler et al., 2003; Urakubo et al., 2003). This suggests that non-synaptic, calcium-induced exocytotic machinery operates in developing cultured neurons.

While it is well established that VRs are ubiquitous neuronal structures, very little is known about their cell biology. Furthermore, the origin and dynamic behavior of the organelles that cluster within VRs are not known. The mechanisms that generate the motility of an entire VR, its splitting and merging behaviors have not been studied. It is unclear whether the organelle clusters within VRs translocate together with the "swollen compartment" or whether they are left behind when the local swelling of the neurite (VR) translocates along. In view of the interconnections between integral membrane proteins and cytoskeletal components of the axoplasm, it is reasonable to assume that giant clusters of organelles cannot translocate as an ensemble within the plasma membrane "sleeve". As mentioned earlier, a number of studies demonstrated that the vesicular content of VRs is competent for fusion with the plasma membrane in response to potassium depolarization. This phenomenon deserves further examination since VRs are motile structures, and it is not clear whether exocytosis can be induced in moving VRs.

In this study, we have used cultured *Aplysia* neurons grown in isolation combined with on-line confocal imaging, retrospective immunofluorescent labeling, electron microscopy and electrophysiological approaches to address these questions.

## Results

### General characterization of the motile behavior and content of VRs formed along neurites

Isolated *Aplysia* neurons in culture form VRs along nascent neurites that extend from the main axon within 4 to 12 h of plating (Fig. 1a). The VRs vary in length from 1.5 to 13 $\mu$m (average $\pm$ s.d.: 5.3 $\pm$ 2.8 $\mu$m; 8 neurons; 387 VRs) and are distributed along the neurites at intervals ranging from 1 to 73.8 $\mu$m (20.5 $\pm$ 13.9 $\mu$m; 6 neurons; 203 VRs). Time-lapse imaging of cultured neurons (once every 4 min, for

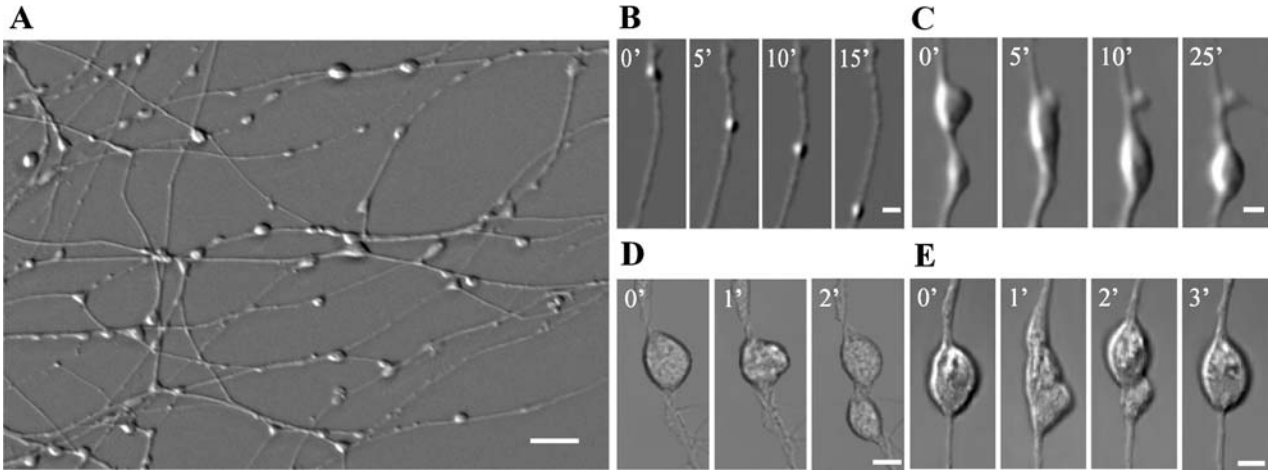


**Fig. 1.** The motile behavior of VRs. A metacerebral neuron was isolated and cultured for 20 h. VRs of different dimensions are seen along the newly formed neurites (a). The formed VRs revealed different forms of motility (video 1). During the sampling period, some of the VRs propagated along the neurites (b) and often fused to form larger VRs (c and video 2). Splitting of VRs to form daughter VRs is also seen (d). The rest of the VRs maintain constant position and wobble in place (e and video 3). Scale bars: (a) 20 $\mu$m, (b–e) 3 $\mu$m.

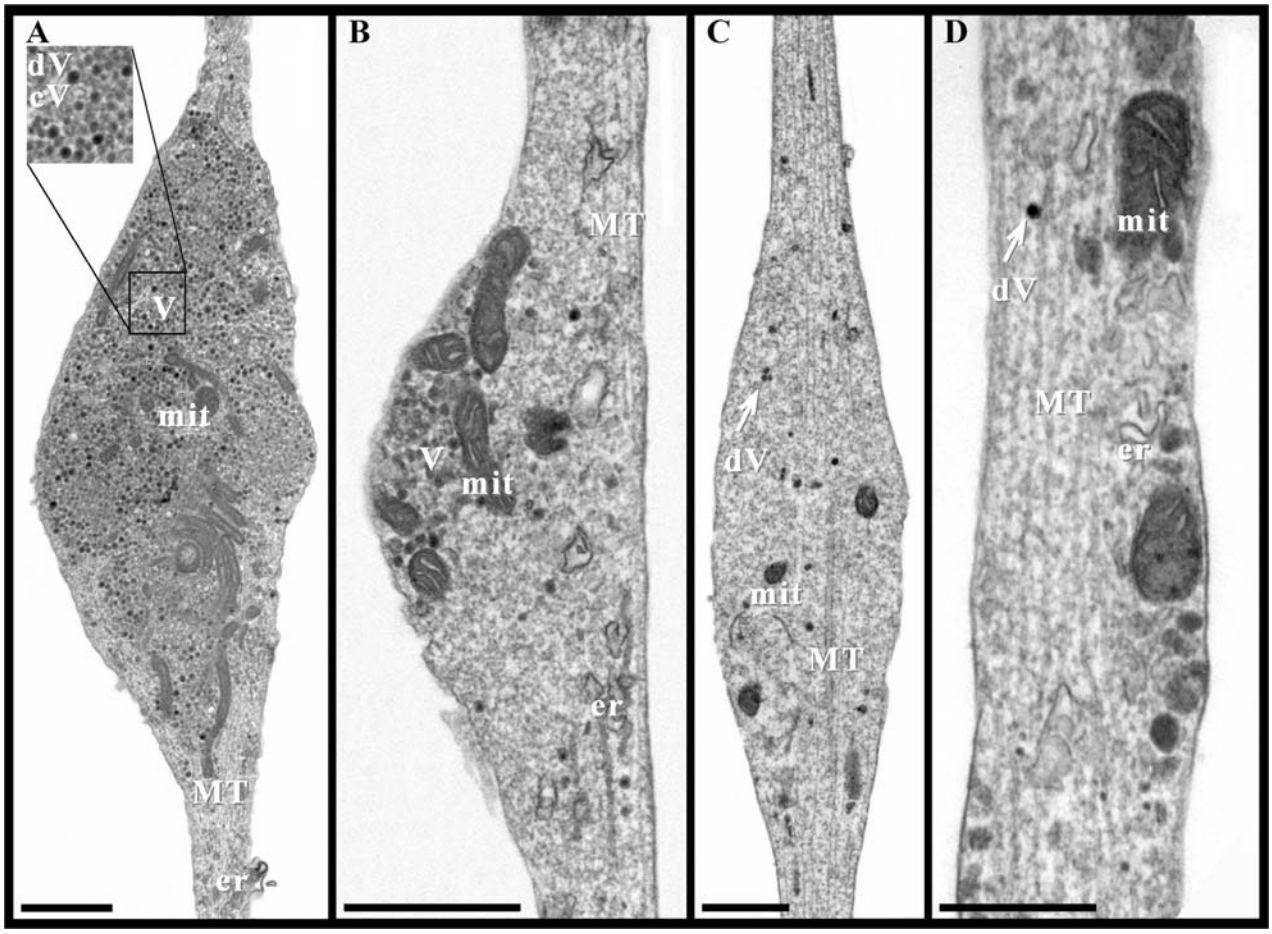


**Fig. 2.** Ultrastructure of VRs and neurites. B neurons were cultured for 24 h, fixed and processed for TEM. The shown micrographs represent the diverse ultrastructural organizations of VRs. (a) A VR highly packed with subcellular organelles. Insert -an enlargement of the square, showing clear and dense core vesicles. (b) A VR containing a single cluster of organelles. (c) A VR devoid of organelles. Note that MTs traverse the length of the VR. (d) A neurite containing vesicles, mitochondria and ER. (V-vesicles; dV- dense core vesicles, cV-clear vesicles, er- endoplasmic reticulum, mit- mitochondria, MT- microtubules. Scale bars: (a–c) 1 $\mu$m, (d) 0.5 $\mu$m.

a period of 40–60 min) revealed a large repertoire of VRs motility (Fig. 1). Within an observation period of 40–60 min, 35.2 $\pm$ 12.9% of the VRs (26 neurons; 2303 VRs) propagated along the neurites (Fig. 1a and video 1) for distances of up to 48 $\mu$m (12.6 $\pm$ 9.6 $\mu$m; 7 neurons; 161 VRs), with a mean propagation velocity of 1.0 $\pm$ 0.8 $\mu$m/min (6 neurons; 93 VRs). Occasionally, VRs switched their direction while propagating. In some cases, motile VRs merged to form larger VRs (Fig. 1c and video 2) or split, yielding a "daughter" VR (Fig. 1d). A large fraction of the VRs (64.7 $\pm$ 12.9%) did not show net translocation; rather they wobbled in place during the observation period (Fig. 1e and video 3).

Electron microscope examination of the VRs content revealed that they contain organelle clusters composed of clear and dense core vesicles, mitochondria, and ER (Fig. 2). In some cases, the clusters appeared to occupy the entire volume of the VR (Fig. 2a), while in other cases they were confined to small, defined areas (Fig. 2b). In most thin sections, longitudinally oriented microtubules (MTs) were observed to extend from one side of a VR to the other (Fig. 2b and 2c). Occasionally, MTs were also found within the periphery of VRs (not shown). As reported earlier (Shepherd and Harris, 1998), a fraction of the VRs were devoid of organelles (Fig. 2c). Clusters composed of a few vesicles (5–20 vesicles), as

well as mitochondria were also observed within thin neurites connecting the VRs (Fig. 2d).

To get a deeper insight into the source of the organelles that cluster within VRs, we differentially labeled Golgi derived, anterogradely transported vesicles and endocytotic vesicles. In addition, to analyze the entire organelle population more comprehensively, all lipid bound organelles were labeled by the styryl dye RH237 (9 neurons, VRs $>$ 50). Thus, 20 h before imaging, freshly cultured neurons were bathed for 30 min in RH237, and the excess dye was washed away. At this point in time the fluorescent dye is distributed among various intracellular organelles (Sahly et al., 2006). Anterogradely transported vesicles were labeled by intracellular injection of mRNA encoding super-ecliptic synaptopHluorin (synpH; Sankaranarayanan et al., 2000) 4–6 h before imaging. The short time interval between mRNA injection and imaging assured that the fluorescent probes labeled almost exclusively newly anterogradely transported vesicles rather than recycled, retrogradely transported plasma membrane. Pinocytotic vesicles were labeled by application of the fluid phase, pinocytotic marker sulfo-rhodamin 101 (SR101) to the bathing solution. Time-lapse images were grabbed either on-line or after the wash. None of these molecular tools noticeably altered the formation or behavior of the VRs.

Using these tools, we found that the vesicle-aggregates within a given VR were composed of Golgi derived vesicles labeled by synpH and endocytotic vesicles labeled by SR101 (Fig. 3a). These vesicles occupied the same domains within the VR. Online imaging revealed that the majority of the SR101 labeled vesicles within a VR were generated by constitutive local pinocytosis. The rest were sequestered into VRs while being retrogradely transported along the neurites. A fraction of the anterogradely transported vesicles was also recruited into the VRs volume. In addition, electron micrographs showed that mitochondria were also incorporated into the vesicle aggregates (Fig. 2).

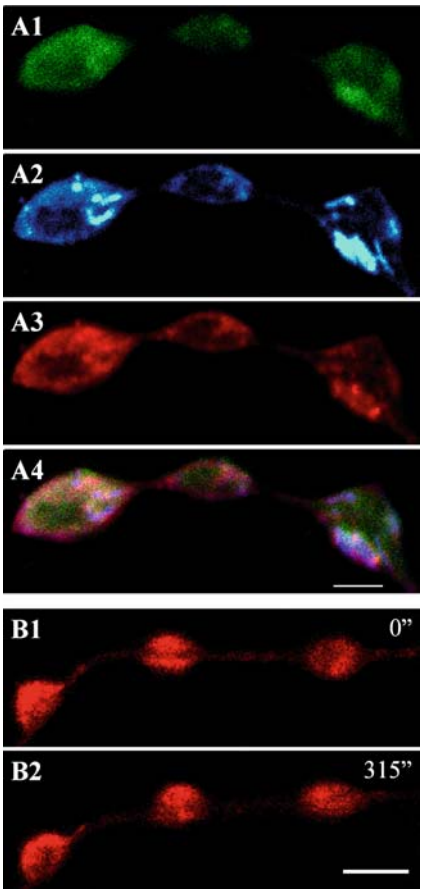


**Fig. 3.** The content, origin and motility of organelles clustered within a VR. (a1) Anterogradely transported vesicles were labeled by synpH (green) and endocytotic vesicles by SR101 (cyan, a2). Note that the Golgi derived and pinocytotic vesicles occupy the same domains within the VR. Non-specific labeling of all membrane bound organelles (including mitochondria) by RH237 (red, a3) is consistent with the conclusion that the organelles occupy the same compartments. (a4) merged image. (b) The spatial distribution of RH237-labeled organelle clusters continuously changes within the VR. Scale bars: (a) 3 $\mu$m, (b) 5 $\mu$m.

**The organelle clusters move along with the VR**

While a number of earlier studies demonstrated that VRs translocate along neurites (Koenig et al., 1985; Hatada et al., 1999, 2000), the mechanisms underlying this phenomenon were not examined. Thus, it is not known whether the organelles clustered within a VR remain stationary while the “swelling” that forms the VR translocates in a peristaltic-like manner, or perhaps the multi-organelle cluster translocates along the neurite as an ensemble within the plasma membrane “sleeve”.

To differentiate between these alternatives we labeled membrane bound organelles by the styryl dye RH237 (19 neurons, VRs $>$ 100) and mitochondria by rhodamine B-[(phenanthren-9-yl)aminocarbonyl]bezyl ester (RPAC) (8 neurons, VRs $>$ 100). The behavior of the RH237-labeled organelles within stationary and motile VRs was imaged 12 to 24 h after application of RH237, at a time point when the fluorescent dye was distributed

among various intracellular organelles (Sahly et al., 2006).

Time-lapse confocal images taken at 45 s intervals revealed that the RH237 labeled organelles clustered within stationary VRs and moved inside the VR volume (Fig. 3b, video 5). In motile VRs, the bulk RH237 labeled organelle clusters translocated together, in concert with the VR (Fig. 4a and 4b and video 4). Occasionally, small RH237 labeled packages broke away and were then transported at a faster rate ($7.9 \pm 6.3\ \mu$m/min, range 1.5 to 26 $\mu$m/min, $n = 6$ cells) along the neurite between VRs (Fig. 4c, arrow). Translocating RH237 labeled organelles occasionally reached nearby VRs and integrated with their content (for example, Fig. 4a).

In a complementary set of experiments we labeled the mitochondria by RPAC and found that mitochondria within VRs translocated in concert with the vesicles (video 6).

The above observations suggest that the organelle clusters, as well as mitochondria, translocate together with the swelling that forms the VR. This conclusion is further supported by labeling of Golgi derived, anterogradely transported vesicles by the photoactivatable-SNAP25 (PA-SNAP25, Patterson and Lippincott-Schwartz, 2002). Twelve to 36 h before the observations, mRNA encoding for the PA-SNAP25 was microinjected into the cell (17 neurons, VRs $>$ 100). Prior to activation of the PA-SNAP25, we verified that no fluorescent signal could be detected along the neurite under study when excited at 488 nm. Then, a single VR was briefly illuminated with the blue laser (405 nm), and as a consequence a green PA-SNAP25 signal could now be detected (Fig. 5a and 5b). In non-motile VRs (wobbling), the activated cytoplasmic PA-SNAP25 signal was retained within the VR for over 30 min, although the signal intensity was reduced due to dispersion of the molecule into the adjacent neurites. In motile or splitting VRs, the activated PA-SNAP25 signal translocated in concert with the VR (Fig. 5b and c and video 7).

In conclusion, the organelle cluster within VRs is comprised of Golgi-derived vesicles, pinocytotic vesicles, and mitochondria. The organelles within an aggregate move in concert with the VR along the neurite. The organelle content of some VRs subdivides into discrete packages that can move independently within the VRs volume or between VRs. In parallel, anterograde and retrograde vesicle transport proceed along the MTs that traverse the VRs, implying that the structure of the VR is not interfering with the MTs based kinesins and dyneins molecular motor functions (Hirokawa and Takemura, 2005).

**Actin packaging of organelle-clusters and its role in VRs motility**

To study the possible role of actin in "enwrapping" the organelle cluster and in its motile behavior, we injected mRNA encoding for actin fused to EGFP (EGFP-actin), 12–24 h before imaging (Sahly et al., 2003; 2006). In a series of observations (19 neurons, VRs $>$ 100), we established that expression of EGFP-actin does not alter the formation of VRs or other characteristic features of the neuron. Confocal time-lapse images taken every 30–60 s revealed that the fluorescent actin signal is not distributed homogeneously along the neurites. Rather, as described by others (Colicos et al., 2001; Sankaranarayanan et al., 2003), occasionally intense EGFP-actin aggregates were present along neurites (video 5). In the VRs, the EGFP-actin appeared to envelop RH237 labeled organelle-clusters (Fig. 4a, B1–B3).

Since the fluorescent EGFP-actin signal was expressed throughout the neurites, it was difficult to determine with certainty whether the actin within a given VR translocated in concert with the organelle aggregates, or whether it stayed in place while the organelles were translocating. To differentiate between these alternatives, we utilized the photoswitchable protein Kaede and fused it to actin (Ando et al., 2002). Kaede emits green fluorescence (515 nm) when excited with a 488 nm laser. After a short illumination with a blue laser (405 nm), the protein loses its emission at 515 nm and emits red fluorescence ($\sim$580 nm) upon excitation with a green laser (543 nm). In a series of observations (11 neurons, VRs $>$ 100) we established that the Kaede-actin fusion protein does not alter the formation and behavior of the VRs whatsoever.

For the experiment, a single VR was imaged in the green channel, to confirm the expression of actin- kaede, followed by imaging in the red channel, verifying that no red signal can be detected prior to the switch (Fig. 6a b1, c1 and 6b b1, c1). Then, the same VR was briefly illuminated with the blue laser and imaged again at both wavelengths. The photoswitched Kaede-actin could now be detected in the red channel (Fig. 6a c2 and 6b c2). Time-lapse images taken every 3 min permitted approximately 15 min of imaging of the switched Kaede-actin. Thereafter, the signal became too weak. During this time course, the green signal, which locally decreased

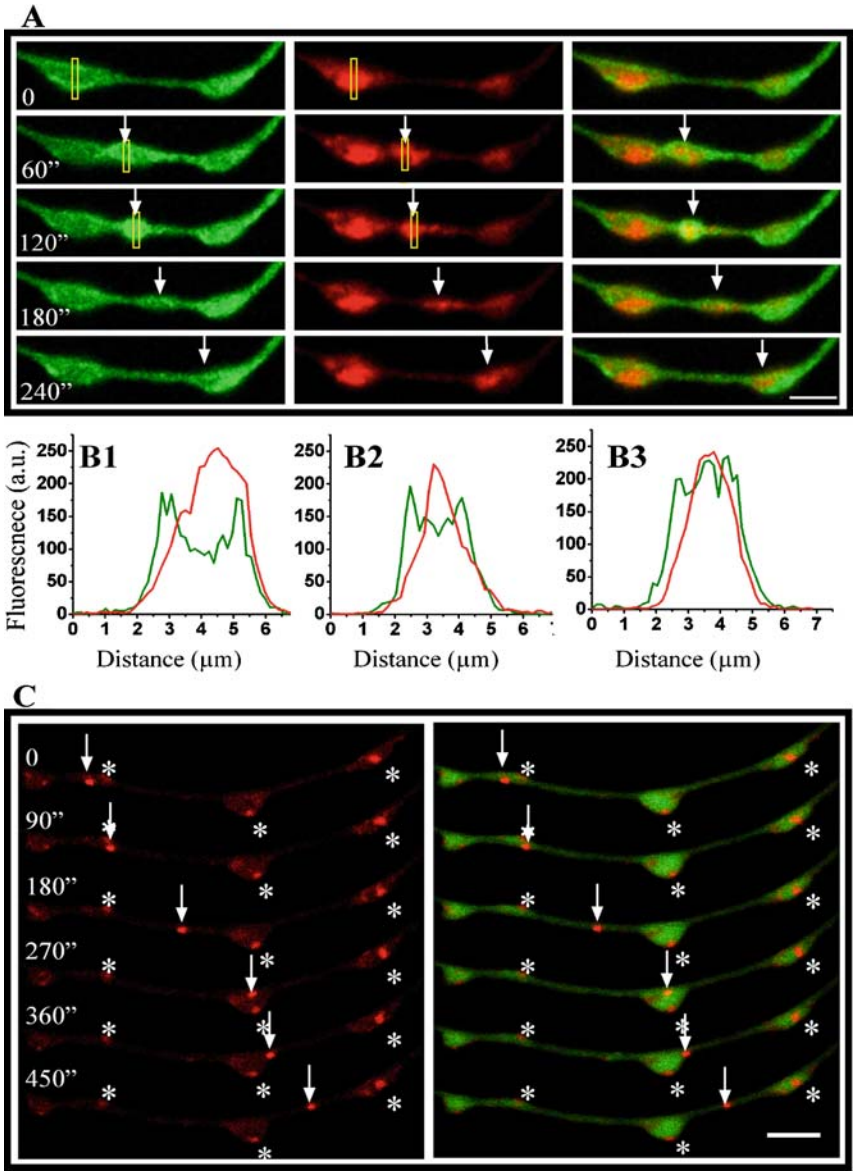


**Fig. 4.** Translocation of organelle clusters along neurites. Neurons were injected with mRNA encoding for EGFP-actin and labeled with RH237. (a) Time-lapse movie taken every 60 s, 0.5 $\mu$m above the substrate level, reveals the translocation of a large fraction of the VR RH237 labeled organelles aggregate. Shown are: actin (green), RH237 (red) and merge images on the right hand side. A large RH237 labeled aggregate surrounded by actin (arrow) moved anterogradely from the VR on the left, and integrated with the contents of the VR on the right, evident by the increase in the RH237 signal there (video 4). (b1–b3) Graph representations of the profiles of the EGFP-actin signal (green traces) and of the RH237 signal (red traces) along the yellow rectangles drawn in (a). b1, b2 and b3 correspond to the top row (0″), the second row (60″) and the third row (120″), respectively. Note that places where the actin signal is low are occupied by a relatively high RH237 signal. (c) Fast translocation of a small RH237-labeled organelle cluster. A neuron was treated similarly to that described in A, and imaged every 45 s. RH237 is shown in red and actin is shown in green (right hand side—a merged image). A relatively small RH237 labeled aggregate (arrow) broke away from the VR on the left hand side of the figure, and moved retrogradely along the neurite. The RH237-labeled package intermittently propagated along the neurite. Asterisks mark stationary RH237-labeled vesicles clusters. Scale Bars: 5 $\mu$m.

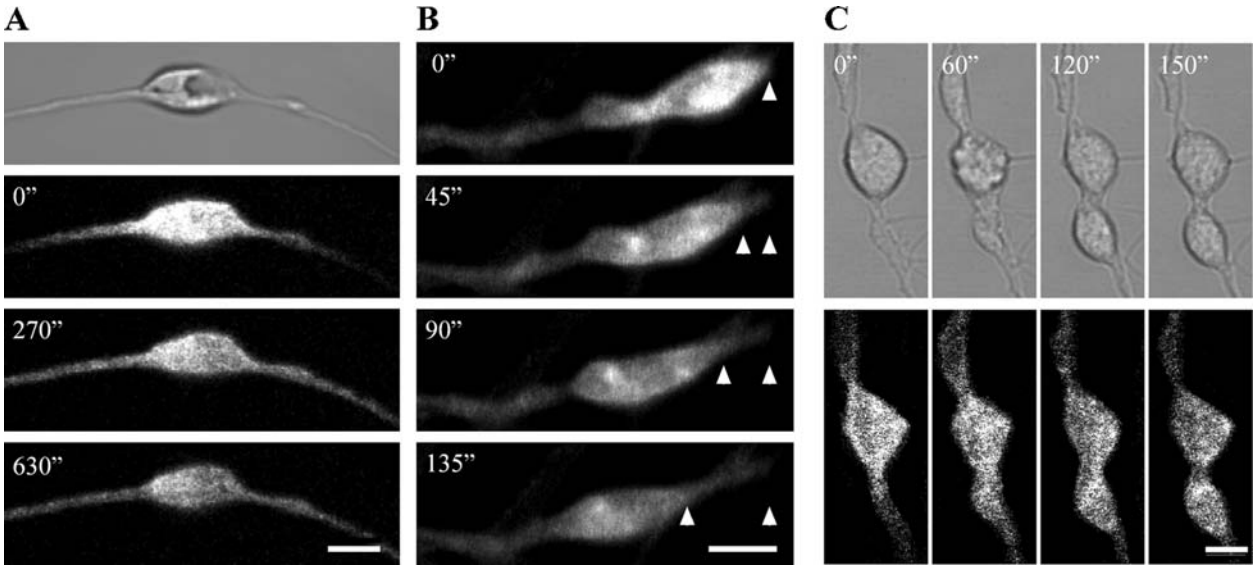


**Fig. 5.** PA-SNAP25 labeled vesicle content moves in concert with the VR. PA-SNAP25 within a single VR was activated and imaged. In stationary VRs, the activated SNAP25 spread bi-directionally into the neurite (a). When a propagating (b) or a splitting (c and video 7) VR was activated, the PA-SNAP25 signal moved along with the VR. (b) Right arrowhead marks the starting point, left arrow head-the new position. (c) A splitting varicosity. Upper row transmitted light micrograph, lower row PA-SNAP25. Scale bars: (a) 5 $\mu$m, (b–c) 3 $\mu$m.

following the switch, recovered (Fig. 6a b2–b5 and (B) b2–b4). Imaging of stationary (wobbling) VRs (Fig. 6a) revealed that the switched Kaede-actin spread slowly from the VR to its surrounding neurite (Fig. 6a c2–c5). In contrast, when a VR translocated along a neurite, its actin contents moved with it (Fig. 6b c2–c4). Furthermore, when a VR split, the actin in the newly formed VR was labeled mainly by switched protein that originated in the "parent" VR (video 8).

We conclude that an actin network within the VR enwraps RH237 labeled organelles (Fig. 4b), and that the actin-organelle complex translocates in synchrony with the VR along the neurite (Figs. 6 and 10).

An earlier study (Sankaranarayanan et al., 2003) revealed that in chemical synapses the actin skeleton acts as a scaffold that retains regulatory molecules such as synapsin. Monoclonal mouse anti-drosophila synapsin antibody that recognizes *Aplysia* synapsin (personal communication, Dr. J. Byrne, University of Texas) was microinjected into the neurons (8 neurons, VRs $>$ 50). 12 to 24 h later, the neurons underwent fixation and were processed to visualize the antibody. Since saponin was used to permeabilize the membrane, we could also use the fixed neurons to image RH237-labeled organelles. As previously described (Angers et al., 2002) the synapsin signal appeared punctated, with higher concentrations in some of the VRs when compared with the adjacent neurites. Similar to the case of chemical synapses, some low synapsin fluorescent signal colocalized with the organelles fluorescence, while higher concentrations were found in regions occupied by actin (Fig. 7a).

### Actin perturbing reagents inhibit VRs translocation

To examine the role of actin in VRs motility, we pharmacologically perturbed the actin structure and imaged the cells once every 4 min for a period of 40 min. Next, one of the actin perturbing drugs: cytochalasin D (10 $\mu$M), latrunculin A (1 $\mu$M), or jasplakinolide (1 $\mu$M) was added to the bathing solution. After an incubation period of a few minutes, an additional time-lapse series of images was taken for 40 min.

Analysis of the data revealed that while in control conditions, 37.7 $\pm$ 6.4% (3 neurons; 181 VRs) of the VRs revealed motility along the neurites, in the presence of 10 $\mu$M cytochalasin D, only 7.0 $\pm$ 4.7% remained motile ($P < 0.05$, paired *t*-test). For latrunculin A, the fraction of motile VRs was reduced from 39.2 $\pm$ 8.1% in the control to 8.0 $\pm$ 4.5% (3 neurons; 244 VRs. $P < 0.05$, paired *t*-test) and for jasplakinolide, from 27.1 $\pm$ 14.3% to 15.9

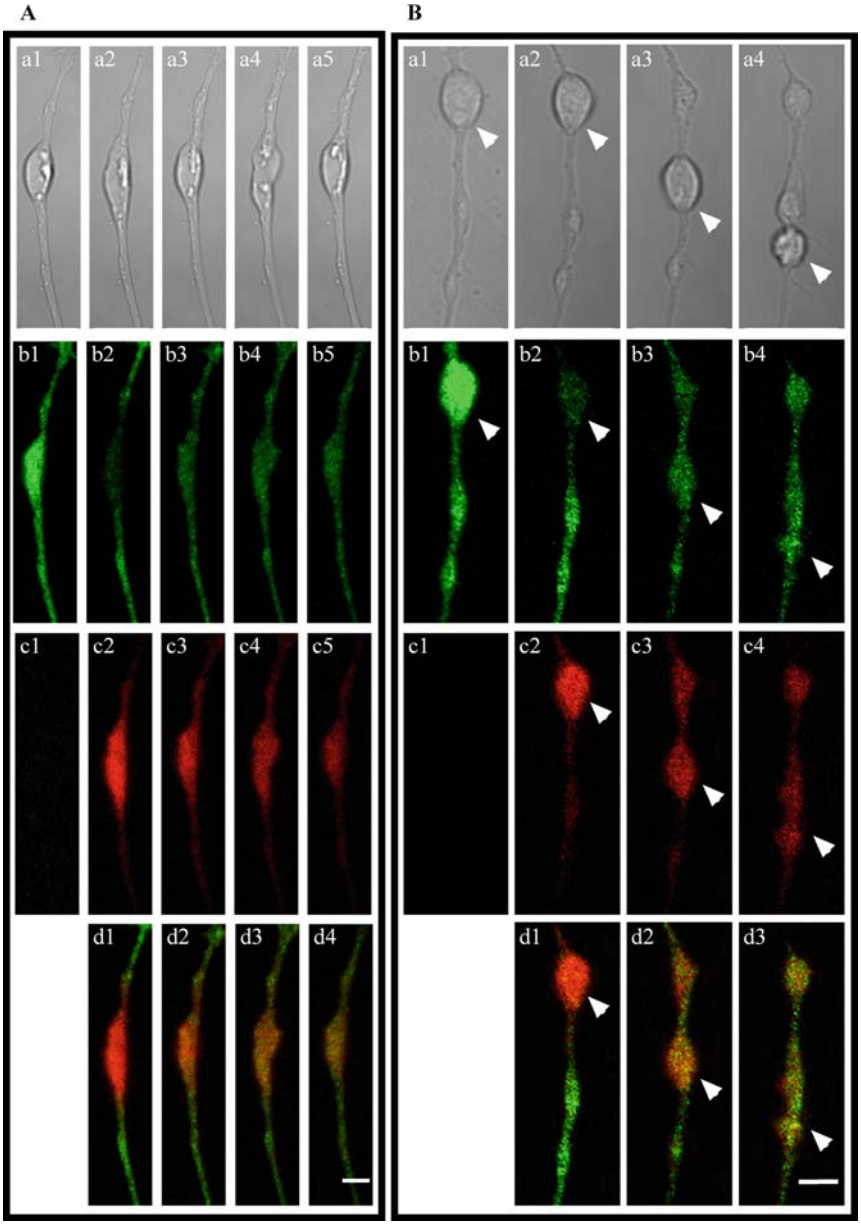


**Fig. 6.** Movement of the actin skeleton in concert with the movement of the VR as revealed by on-line Kaede-actin imaging. Shown are examples of a stationary (wobbling) VR (a), and of a motile VR (b). In both types of experiments the VRs were first imaged in the green wavelength to confirm the expression of Kaede-actin by the neuron (a-b1 and b-b1), and then in the red wavelength, to confirm that no signal is generated in this channel (a-c1 and b-c1). Then, in each experiment the VR under study was illuminated briefly with a blue laser (405 nm) to photo-switch the Kaede to red, and imaged again at the two wavelengths (a-b2, c2 and b-b2, c2). Note that concomitantly with the decrease in the green signal (compare a-b1 with a-b2, and b-b1 with b-b2, arrowhead) the red signal within the switched VRs increased (compare a-c1 with a-c2, and b-c1 with b-c2, arrowhead). The shown images are taken from time-lapse movies taken every 3 min. In stationary (wobbling) VRs, such as the one shown in (a), the switched actin spread out of the VR into the neurite in both directions (a-c2, c3, c4). In the motile VR shown in (b), 3–9 min after switching (b-c2, c3, c4, arrowhead), the translocation of the VR was accompanied by the translocation of the switched Kaede-actin, while a fraction of the switched actin remains behind as the VR translocates. (a-d1-4 and b-d1-3) are merged images. Scale bars: 5 $\mu$m.

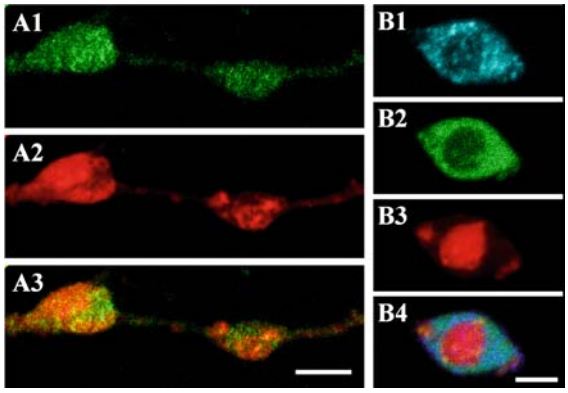


**Fig. 7.** Synapsin and myosin II immunolabeling. (a) Synapsin immunolabeling. Synapsin is distributed throughout VRs as puncta in a rather inhomogeneous manner. It is also detectable at lower levels along neurites (not shown). Labeling of lipid bound organelles with RH237 reveals a reciprocal distribution of synapsin (a1) and vesicles (a2). (a3) Merged image. Scale bar 5 $\mu$m. (b) Non-muscle Myosin II is distributed in a punctated form along neurites with a higher concentration within VRs, especially in their perimeter (cyan, b1). Actin filaments, labeled by fluorescein-phalloidin, occupy the same compartment as the myosin (green, b2). Post fixation labeling of membranous organelles with RH237 (red, b3) revealed that clusters of membrane bound organelles are enwrapped by actomyosin envelope. (b4) Merged image. Scale bar: 3 $\mu$m.

$\pm$ 10.8% (6 neurons; 526 VRs. $P < 0.01$, paired *t*-test). The drug-induced reduction in the VRs motility was not correlated with the dissociation of the organelle aggregates. This suggests that, as in synaptic terminals, the actin network enwraps the clusters, but does not hold them together (Sankaranarayanan et al., 2003).

**Myosin II and VRs motility**

The non-muscle myosin II molecular motor, which binds and contracts actin filaments, has been demonstrated to play an important role in generation of synaptic vesicles translocation as well as motility of spines and GCs in various neuronal systems (Ryan, 1999; Medeiros et al., 2006; Ryu et al., 2006). This prompted us to examine whether, in addition to mechanical force generation by actin polymerization and depolymerization, the motile behavior of VRs is also related to actomyosin machinery. We therefore applied 100 $\mu$M blebbistatin, a specific inhibitor of myosin II ATPase activity (Straight et al., 2003), to the bathing solution. This decreased the percentage of motile VRs from 42.1 $\pm$ 19.5% to 20.0 $\pm$ 4.7% (5 neurons; 418 VRs. $P < 0.01$-paired *t*-test), indicating that myosin is involved in VRs motility.

To investigate the spatial relation between the actin network and myosin motors, we next immunolabeled myosin II with an antibody raised against *Aplysia* myosin (Medeiros et al., 2006). In addition to the classical method of processing immunolabeling, and to assure good distribution of the primary antibody, we injected the myosin II antibody into the cell body cytoplasm (9 neurons, VRs $>$ 100), and 12 h later, the neurons were processed to dissolve the plasma membrane and stabilize the cytoskeleton (Medeiros et al., 2006). This procedure dissociates and washes away non-cytoskeleton associated proteins (Nakhost et al., 2002), including soluble myosin forms and G-actin, leaving the bound myosin and F-actin in place. The primary myosin antibody was then decorated by the secondary antibody, and the actin filaments were labeled by fluorescein-phalloidin. Myosin labeling was noticeable mainly within VRs and to a lesser extent within the neurites. In some VRs the myosin appeared to concentrate at the perimeters of the cytoplasm (Fig. 7b1), while in others, labeling was homogenously distributed. Some VRs hardly revealed a myosin signal. The phalloidin fluorescence was either homogenously distributed within the VRs or contained empty pockets (Fig. 7b2). To better understand the spatial relationships between myosin, the phalloidin pockets and membranous organelles, we immunolabeled the myosin and actin using a more gentle procedure (saponin instead of triton), and labeled lipid bound organelles by RH237. We found the RH237 labeled organelles to be enwrapped by an actin filament network which contained myosin (Fig. 7b3).

Taken together, the pharmacological effects of blebbistatin, and actin perturbing reagents, as well as fluorescent labeling, suggest that actin and myosin both are involved in generating the motility of the VRs.

**Calcium-dependent fusion of vesicles with the VRs plasma membrane**

Evoked neurotransmitter release from neurons is typically associated with a highly organized presynaptic apparatus that includes clustering of voltage gated calcium channels (VGCCs; Sudhof, 2004), assembly of the presynaptic molecular complex, and concentration of release competent vesicles (Waites et al., 2005). The observations that VRs wobble and translocate along neurites, combined with the fact that their vesicular content does not

maintain a constant position in respect to the plasma membrane, raise the question whether they exhibit evoked exocytosis.

To examine this possibility, we labeled Golgi derived vesicles by injecting mRNA encoding synpH. Imaging of synpH-expressing neurons, by excitation at 488 nm, 12 h after the injection, revealed some signal on the plasma membrane and a low signal within the neurites and VRs (Fig. 8a). Imaging the same VRs with a 405 nm laser (synpH facing the acidic lumen of vesicles), revealed clusters of synpH throughout the region (Fig. 8, compare b and c). The neuron was then intracellularly stimulated to fire trains of action potentials (APs). Simultaneously, the fluorescent signals generated by synpH were imaged by excitation at 488 nm and 405 nm, revealing the synpH that fuses with the plasma membrane and faces the neutral pH of the medium (Fig. 8b and 8d), and synpH that faces the acidic lumen of the vesicles. We found that stimulation with a train of APs led to fusion of vesicles with the plasma membrane in 88 out of 191 VRs examined (8 neurons). It should be noted that only signal increases greater than 10% were counted, so that it is possible that AP-induced fusion took place in a larger fraction of VRs. The average rise in the signal was 35 $\pm$ 30%.

The fusion of vesicles with the plasma membrane was associated with a rise in the $[Ca^{2+}]_i$, as evidenced by Rhod-2 imaging (Fig. 8f and 8g). On stimulation, the Rhod-2 signal increased throughout the cytoplasm of the axon and neurites, including the VRs. The temporal resolution used by us revealed that the rise in $[Ca^{2+}]_i$ was faster than the rise in the synpH signal by a factor of 2.4 $\pm$ 1.3 (Fig. 8g). The synpH decay time was 71 $\pm$ 30 s. Both the rise in calcium and the subsequent exocytosis were inhibited by the VGCC-blocker nitrendipine. To ensure that we were observing exocytosis, an acidic solution (pH 5.5) was ejected through a nearby micropipette onto the VRs. Application during the train of APs revealed a reversible drop in the synpH signal without affecting the calcium signal (data not shown). These experiments suggest that VGCCs are expressed all over the plasma membrane of the neurites, and that the elevation in $[Ca^{2+}]_i$ leads to exocytosis which is followed by membrane retrieval. The release was observed in approximately half of the VRs (Fig. 8d and 8g).

Since Rhod-2, as well as other calcium indicators, may act as a carrier that mobilizes the calcium within the cytosol (Gabso et al., 1997) and thus may generate a misleading impression in terms of the spatial distribution of the VGCCs, we complemented the Rhod-2 calcium imaging experiment with EGFP-DOC2, which is less mobile than Rhod-2 (Malkinson and Spira, 2006). Upon binding of calcium to the C2 domain, EGFP-DOC2 translocates from the cytosole to the plasma membrane. Using EGFP-DOC2 we confirmed the Rhod-2 observations, namely that VGCCs are embedded all along the neurites plasma membrane. Interestingly, we also observed spontaneous translocations of DOC2 in VRs, indicating local rises in $[Ca^{2+}]_i$ (not shown).

To examine whether a moving VR maintains its ability to exhibit $[Ca^{2+}]_i$ induced exocytosis, neurons were labeled with either DOC2B or synpH (5 and 9 neurons, respectively. VRs $>$ 50), as described above. The neurons were stimulated to fire APs every few frames, while a VR was translocating along a neurite. These experiments revealed that firing of APs elevated the $[Ca^{2+}]_i$ and induced exocytosis while the VRs were moving from one location to another (Fig. 9 and videos 9, 10). In conclusion, AP-induced calcium influx in translocating VRs leads to exocytosis followed by endocytosis.

## Discussion

Confocal imaging of VRs formed along neurites of cultured *Aplysia* neurons revealed that VRs host a heterogeneous population of subcellular organelles that include clear and dense core vesicles, mitochondria and ER. The number and composition of the organelles within a VR varies continuously. Small packages break off from the cluster and are retrogradely or anterogradely transported, at a significantly faster rate than the VR moves (7.9 $\pm$ 6.3 $\mu$m/min; 1.0 $\pm$ 0.8 $\mu$m/min, respectively). The entire VR, including its content, intermittently translocates at an average speed of 1.0 $\pm$ 0.8 $\mu$m/min along neurites within the plasma membrane "sleeve". VRs fuse with each other or split to form daughter VRs. The composition of the organelle population within VRs is dynamic. Constitutive local membrane retrieval adds pinocytotic vesicles to the cluster (Fig. 10a #1). Anterogradely (Fig. 10a #2) and retrogradely transported vesicles (Fig. 10a #3) and mitochondria are also sequestered to the cluster. The composition of organelles content of individual VRs is further altered by transport of organelle clusters that break away from one VR and are transported to another. Similar

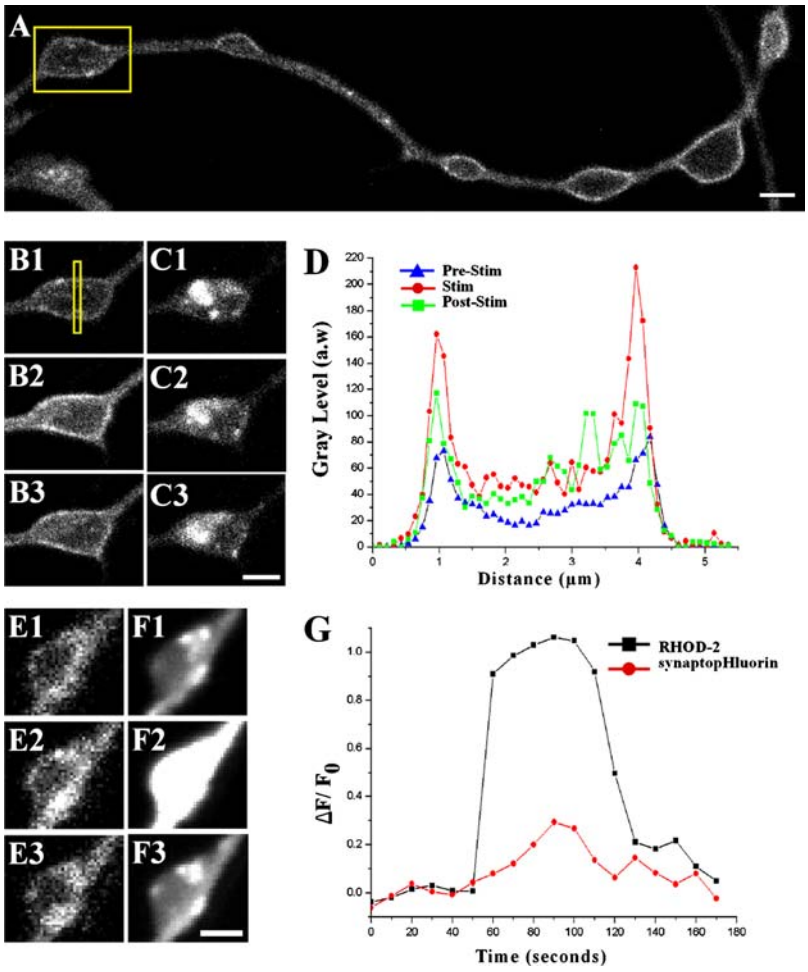


**Fig. 8.** Activity-induced elevation of $[Ca^{2+}]_i$ within VRs leads to exocytosis, followed by membrane retrieval. A neuron expressing synpH was loaded with the calcium indicator Rhod-2. (a) Excitation with a 488 nm laser reveals synpH fluorescence on the membrane of the VRs and along the neurite. (b, c) Enlargements of the VR marked by a yellow rectangle in (a). Following a train of APs evoked by a stimulating microelectrode, exocytosis of synpH-labeled vesicles occurs as revealed by the increase in the synpH signal mainly on the membrane, followed by membrane retrieval. Images b1–b3 were taken with the 488 nm laser, at time intervals of 140 s. b1, b2 and b3- before, during and after stimulation, respectively. Images c1–c3 were taken with the 405 nm laser at the same time-points as b1–b3. The change in the signal during the stimulation was minor (not shown). (d) A graph representing the change in the fluorescent signal intensities collected with the 488 nm laser inside the yellow rectangle in b1. The traces in the graph correspond to images b1–b3. e1–e3 show the synpH signal at 488 nm in a different VR before, during and after a train of APs, respectively. Images were taken at time intervals of 80 s. A clear increase in the synpH fluorescent intensity can be seen in e2 and the recovery in e3. f1–f3 were taken at the same time-points and depict the Rhod-2 fluorescent signal. (g) The graph shows the results of the experiment from which the images in (e, f) were taken. Scale bars: (a, c3) 3 $\mu$m, (F3) 2 $\mu$m.

sharing of vesicles among neighboring presynaptic boutons was recently reported to take place in rat hippocampal neurons (Darcy et al., 2006). Electron micrographs and confocal imaging revealed the presence of VRs that are devoid of vesicles. Thus, we assume that, at least transiently, the characteristic swelling that morphologically defines a VR can be maintained in the absence of the organelle-clusters.

Through the use of GFP-actin, Kaede-actin and phalloidin-FITC, in combination with vesicles labeled by RH237 or PA-SNAP25, we found that an actin network enwraps the clusters of organelles within a VR (Fig. 10a #4). Since the enwrapping actin was stained by phalloidin-FITC and resisted washout after membrane permeabilization, it is reasonable to assume that it is in filamentous form. Furthermore, we have documented the concerted

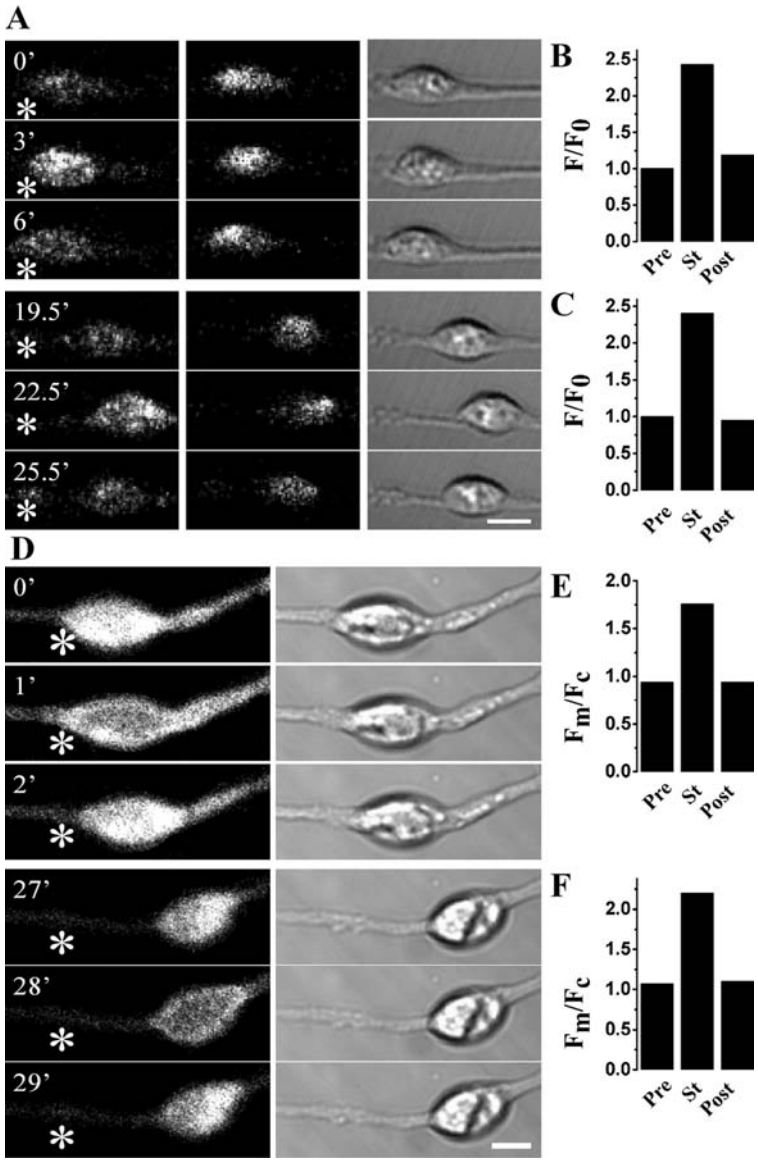


**Fig. 9.** Elevation of the calcium concentration and exocytosis in moving VRs. (a) A neuron expressing synpH was imaged with the 488 nm laser (left column) and sequentially with the 405 nm laser (middle column). It was then impaled with a stimulating microelectrode. Images were taken from a time-lapse movie, of a moving VR. 0′, 3′ and 6′ are images taken at its first location before, during and after a train of APs, respectively. After the VR has covered a substantial distance (19.5′) and while it was still in motion, a second train of APs was applied, and a rise in the signal was again detected (22.5′), followed by signal recovery (25.5′) (video 10). The bars in (b, c) depict the VR signal generated by the 488 nm laser at the first (b) and second locations (c). Shown are the results of the average intensity of an area of interest (AOI) around the VR before the stimulation (left bar, pre), during the stimulation (middle bar, st) and the recovery (right bar, post). (d) A neuron expressing EGFP-DOC2B was impaled with a stimulating microelectrode. Images were taken from a time-lapse movie of a moving VR. 0′, 1′ and 2′ are images taken at its first location before, during and after a train of APs. Note the translocation of DOC2B to the membrane during the stimulation. After the VR covered a substantial distance (27′) and while it was still in motion, a second train of APs was applied (28′), causing translocation of the DOC2B to the membrane. The bars in (e, f) depict the VR signal generated by the 488 nm laser at the first (e) and second locations (f). Shown are the ratios resulting from division of the membrane AOI signal by the cytosolic AOI signal before the stimulation (left bar), during the stimulation (middle bar) and the recovery (right bar). Asterisks in images (a) and (d) mark the original positions of the VRs. Scale bars: (a) 3 $\mu$m, (b) 5 $\mu$m.

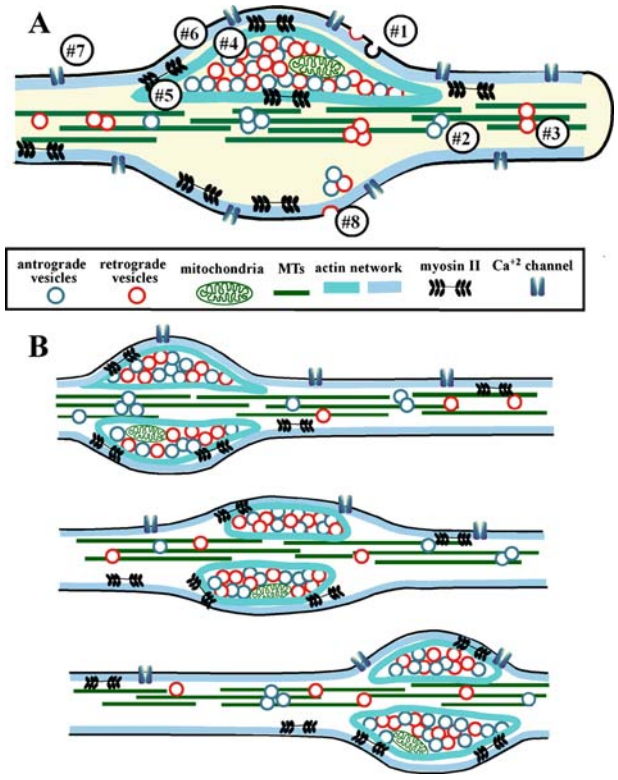


**Fig. 10.** A model for VRs structure and motility. For details see Discussion.

movement of vesicles and the enwrapping actin network. Thus, we propose that, as in the case of hippocampal synaptic terminals, actin, possibly in concert with synapsin, serves as a scaffold that holds the vesicles in a cluster (Sankaranarayanan et al., 2003).

We interpret our images to suggest that the packaged organelles within the actin scaffold translocate in respect to the plasma membrane "sleeve" (Fig. 10b). Mobile actin packets have been reported to traverse along the axons of rat hippocampal neurons. It was suggested that these packets were formed by budding off of presynaptic actin, and could later serve as the cytoskeletal basis for new presynaptic regions (Colicos et al., 2001).

The findings that the cytoskeleton-perturbing drugs cytochalasin D (10 $\mu$M), latrunculin A (1 $\mu$M), and jusplakinolid (1 $\mu$M) interfere with the directional motility of the VRs is consistent with the view that actin networks are involved in the translocation of the VRs (Fig. 10b). The presence of myosin II within the VRs cytoplasm (Fig. 10a #5), and the findings that blebbistatin greatly reduces VRs motility suggest that myosin is involved. Based on earlier studies which relate motility of growth cones, spines and synaptic vesicles to actomyosin complexes (Ryan, 1999; Medeiros et al., 2006; Ryu et al., 2006), we tentatively suggest that wobbling of VRs is generated by continuous local actomyosin contraction. Vectorial translocation is generated by the same molecular mechanisms, but the force is generated between a stable sub-membrane actin network and the actin network that enwraps clusters of vesicles (Fig. 10a #6 and #4, respectively and 10b). It should be noted that the mechanisms of cluster translocation within a plasma membrane sleeve are independent of the formation of adhesion plaques that anchor the plasma membrane and the culture substrate. Consistent with this is the observation that VRs do not form adhesion plaques with the substrate. It is likely that the non-polarized nature of the actin scaffold underlies the bidirectional nature of the VRs motility. We further suggest that the breaking off of small clusters of vesicles may be generated by myosin II, yet once the vesicles or the small clusters come into contact with the MTs, the translocation is faster and most likely generated by the kinesin and dynein molecular motors (Hirokawa and Takemura, 2005).

A number of investigators demonstrated that elevation of the $[Ca^{2+}]_i$ in cultured neurons induces exocytosis from axonal shafts, growth cones and VRs, implying that potassium depolarization is sufficient to induce vesicles release from non-synaptic structures before the establishment of contact with postsynaptic elements (for references see introduction).

In the present study we found that all VRs examined revealed an increased $[Ca^{2+}]_i$ in response to trains of action potentials. Since nitrendipine inhibited the AP-induced elevation of $[Ca^{2+}]_i$, we conclude that the elevation is generated by influx of calcium through VGCCs (Fig. 10a #7). Furthermore, imaging of $[Ca^{2+}]_i$ by DOC2 translocation (Malkinson and Spira, 2006) suggests that the increase in $[Ca^{2+}]_i$ does not reflect fast mobilization of calcium by the indicator (Gabso et al., 1997), but rather reflects the localized influx through the plasma membrane. This conclusion accounts for the observation that repeated stimulation elevates the $[Ca^{2+}]_i$ within the VR while it propagates. Nevertheless, approximatly 50% of the VRs which host synpH labeled vesicles revealed exocytosis (Fig. 10a #8) in response to the elevation in $[Ca^{2+}]_i$. It should be noted that this number is an underestimate because of a signal to noise problem

associated with using synpH. If the size of the vesicle pool in the non-responsive VRs was too small, than the signal associated with exocytosis could be eclipsed by the presence of surface synpH. In any case, a simple interpretation of this observation is that the probability of the vesicles to be in close apposition with the plasma membrane is about 0.5. It should be noted that metacerebral and buccal neurons form slow releasing synapses (Schacher, 1985; Whim et al., 1997), thus it is likely that the observed release represents the mature form of a slow synapse. An alternative explanation is that the molecular mechanisms underlying vesicles fusion with the VRs plasma membrane are not fully assembled in some of the VRs.

The functional roles of VRs are not known; they could serve as suggested above, as prefabricated "ready to go" presynaptic boutons and thus facilitate synaptogenesis. In such a case, VRs motility may be advantageous in increasing the probability of a VR to come into close physical contact with potential postsynaptic sites. Alternatively, VRs could be an epiphenomenon of developmental processes in which excess organelles and molecules are temporarily stored until a steady state of the neuron is reached. These questions will be addressed by presenting potential postsynaptic neurons to VRs and directly studying the outcome of such interactions.

## Methods

### Cell culture

Neurons B1 and B2 from buccal ganglia and metacerebral neurons (MCn) from the cerebral ganglia of *Aplysia californica* were isolated and maintained in culture as previously described (Schacher and Proshansky, 1983; Spira et al., 1996). In the present study we refer to the buccal neurons collectively as B neurons.

### Culture medium

The culture medium consisted of 10% filtered hemolymph obtained from *Aplysia facciata* diluted in modified Leibovitz's L 15 Medium as previously described (Spira et al., 1996).

### Chemicals and pharmacological reagents

RH237 (N-(4-sulfutyl)-4-(6-(p-dibutylamynophenyl) hexatrenyl)) pyridinum, inner salt, a gift from Dr. R. Hildeshiem, the Weizmann Institute of Science (Grinvald et al., 1982), was diluted in ethanol to a concentration of 10 mM and further diluted before use in artificial sea water (ASW) to a concentration of 15–20 $\mu$M. Sulforhodamine 101 (SR-101, Kodak) was prepared as a stock solution of 10 mM in double distilled water and further diluted before use in ASW to a final concentration of 40 $\mu$M.

5 mM jasplakinolide (Molecular Probes), or 10 mM cytochalasin D (Sigma) DMSO stock solutions were dissolved in ASW to concentrations of 1 $\mu$M and 10 $\mu$M, respectively. Blebbistatin and nitrendipine (Sigma, Israel) were prepared as 100 mM and 50 mM stock solutions in DMSO, respectively, and dissolved in the experimental dish to a final concentration of 100 $\mu$M.

Rhodamine B-[(phenanthren-9-yl) aminocarbonyl]bezyl ester (RPAC- a gift from Prof. Ioav Cabantchick, The Hebrew University) was prepared as a 3.84 mM stock solution in DMSO, and further diluted in the experimental dish to a final concentration of 0.5 $\mu$M. Rhod-2 was loaded into the cells as described previously (Malkinson and Spira, 2006).

### mRNA preparation and injection

mRNAs were in vitro transcribed using the recombinant transcription system, as described by our laboratory (Sahly et al., 2003). EGFP-Actin (provided by Dr. DesGrosiller, Montreal University), PA-SNAP25 (a gift from Prof. George Augustine), Kaede-Actin (Bioconsult) and super ecliptic synaptopHluorin (provided by Dr. James E. Rothman, Sloan-Kettering Inst.) were cloned in pCS2+ expression vector and the transcribed mRNAs were pressure-injected into the cytoplasm of the cultured neurons 4–24 h after plating, as described by Sahly et al. (2003).

### Immunochemistry

Myosin antibody (polyclonal rabbit anti-aplysia myosin II, a gift from Prof. Paul Forscher, Yale University) retrospective immunolabeling was performed as previously described by Medeiros et al. (2006) with sheep anti-rabbit IgG, Cy3 conjugated, Sigma; 1:500 dilutions and phalloidin-FITC (Sigma). Synapsin antibody (monoclonal mouse anti Drosophila Synapsin antibody, developed by Erich Buchner, was obtained from the Developmental Studies Hybridoma Bank developed under the auspices of the NICHD and maintained by The University of Iowa, Department of Biological Sciences, Iowa City, IA 52242)

retrospective immunolabeling was performed as described by Gitler and Spira (1998) with the following modifications:

To improve the distribution of the primary antibodies in some experiments we pressure injected the diluted $\alpha$-myosin (1:20), or $\alpha$-synapsin into the neurons. In these experiments the fixation was carried out 12–24 h after the injection. In the shown figure (Fig. 7) we immunolabeled the myosin and actin as described above, without dissolving the lipid membrane in triton, but rather by a delicate permeabilization procedure using saponin (Gitler and Spira, 1998). A few minutes before imaging, RH237 was added to the culture dish to a final concentration of 1.25 $\mu$M.

**Confocal microscope imaging**

The systems used for confocal imaging consisted of a Nikon C1 confocal system mounted on a Nikon TE-2000 Eclipse microscope system with a Nikon plan-Apo chromat 60$\times$1.4 NA oil objective. This system is equipped with 3 lasers: blue diode (405 nm), Argon (488 nm) and Green HeNe (543 nm). Images were collected and processed using EZ-C1 software. The system used for confocal imaging of EGFP-DOC2B consisted of an Olympus microscope IX70 and a Bio-Rad Radiance 2000/AGR-3 confocal imaging system. The objective used was an Olympus planApo 60$\times$1.4 NA oil objective. The protein was excited with 488 nm (Argon laser), emission collected at 500–560 nm. The images were collected using LaserSharp.

RH237 was excited with the 488 nm laser, and the emission was collected through 610LP filter. EGFP-Actin was excited with the 488 nm laser and the emission was collected with 515/30. PA-SNAP25 was activated by placing a 256 pixel $\times$ 256 pixel square, with dimensions of typically 10 $\mu$m $\times$ 10 $\mu$m, over the VR and illuminating it once with 10 nanoseconds dwell time with the 405 nm laser. It was then excited with the 488 nm laser. Emission was collected with 515/30. Kaede-Actin was switched similarly, but was then excited sequentially with the 488 nm laser and the 543 nm laser. The emissions were collected sequentially with 515/30 and 605/75, respectively. SynpH was excited with 405 nm or 488 nm and collected with 515/30. Images were analyzed off line using NIH ImageJ software (Bethesda, MD). The figures were prepared using Adobe Photoshop and Macromedia FreeHand software.

For demonstration of the average intensity along the rectangles in Fig. 4(A), a 3-pixel wide rectangle was drawn on the relevant region, and its average profile was plotted using ImageJ. For calculation of $F_0$ in Fig. 9(A), the average of the three images prior to each of the two stimulations was calculated separately.

For stimulation of the cells, glass electrodes were pulled to resistances of $\sim$7–10 M$\Omega$, and filled with 2 M KCl solution. The synpH-expressing cells, were electrically stimulated by intermittent depolarizing square pulses delivered at intervals of 60 milliseconds for approximately one minutes, at a frequency of 8 Hz. For stimulation of DOC2-expressing cells, intermittent depolarizing square pulses were delivered at intervals of 50 milliseconds for approximately 15 s, at a frequency of 18 Hz.

**Electron microscopy**

Electron microscopy was performed as previously described by our laboratory (Spira et al., 2003).

## Acknowledgments

This study was supported by grants from the USA-Israeli Bi-national Science Research Foundation (2000354 and 2003152). Parts of the work were done at the Charles E. Smith Family Laboratory for Collaborative Research in Psychobiology. Funding of this project was refused by the Israel Science Foundation. M.E. Spira is the Levi DeViali Prof. in Neurobiology.

## References

Ando, R., Hama, H., Yamamoto-Hino, M., Mizuno, H., and Miyawaki, A. (2002). An optical marker based on the UV-induced green-to-red photoconversion of a fluorescent protein. Proc. Natl. Acad. Sci. USA *99*, 12651–12656.

Angers, A., Fioravante, D., Chin, J., Cleary, L. J., Bean, A. J., and Byrne, J. H. (2002). Serotonin stimulates phosphorylation of Aplysia synapsin and alters its subcellular distribution in sensory neurons. J. Neurosci. *22*, 5412–5422.

Cibelli, G., Ghirardi, M., Onofri, F., Casadio, A., Benfenati, F., Montarolo, P. G., and Vitiello, F. (1996). Synapsin-like molecules in Aplysia punctata and Helix pomatia: Identification and

distribution in the nervous system and during the formation of synaptic contacts *in vitro*. Eur. J. Neurosci. *8*, 2530–2543.

Colicos, M. A., Collins, B. E., Sailor, M. J., and Goda, Y. (2001). Remodeling of synaptic actin induced by photoconductive stimulation. Cell *107*, 605–616.

Dai, Z. and Peng, H. B. (1996). Dynamics of synaptic vesicles in cultured spinal cord neurons in relationship to synaptogenesis. Mol. Cell. Neurosci. *7*, 443–452.

Darcy, K. J., Staras, K., Collinson, L. M., and Goda, Y. (2006). Constitutive sharing of recycling synaptic vesicles between presynaptic boutons. Nat. Neurosci. *9*, 315–321.

Fiumara, F., Onofri, F., Benfenati, F., Montarolo, P. G., and Ghirardi, M. (2001). Intracellular injection of synapsin I induces neurotransmitter release in C1 neurons of Helix pomatia contacting a wrong target. Neuroscience *104*, 271–280.

Gabso, M., Neher, E., and Spira, M. E. (1997). Low mobility of the $Ca^{2+}$ buffers in axons of cultured Aplysia neurons. Neuron *18*, 473–481.

Gitler, D. and Spira, M. E. (1998). Real time imaging of calcium-induced localized proteolytic activity after axotomy and its relation to growth cone formation. Neuron *20*, 1123–1135.

Grabham, P. W., Wu, F., Schacher, S., and Goldberg, D. J. (2005). Initiating morphological changes associated with long-term facilitation in Aplysia is independent of transcription or translation in the cell body. J. Neurobiol. *64*, 202–212.

Grinvald, A., Hildesheim, R., Farber, I. C., and Anglister, L. (1982). Improved fluorescent probes for the measurement of rapid changes in membrane potential. Biophys. J. *39*, 301–308.

Hatada, Y., Wu, F., Silverman, R., Schacher, S., and Goldberg, D. J. (1999). En passant synaptic varicosities form directly from growth cones by transient cessation of growth cone advance but not of actin-based motility. J. Neurobiol. *41*, 242–251.

Hatada, Y., Wu, F., Sun, Z. Y., Schacher, S., and Goldberg, D. J. (2000). Presynaptic morphological changes associated with long-term synaptic facilitation are triggered by actin polymerization at preexisting varicositis. J. Neurosci. Online *20*, Rc82.

Hirokawa, N. and Takemura, R. (2005). Molecular motors and mechanisms of directional transport in neurons. Nat. Rev. Neurosci. *6*, 201–214.

Koenig, E., Kinsman, S., Repasky, E., and Sultz, L. (1985). Rapid mobility of motile varicosities and inclusions containing alpha-spectrin, actin, and calmodulin in regenerating axons *in vitro*. J. Neurosci. *5*, 715–729.

Kraszewski, K., Mundigl, O., Daniell, L., Verderio, C., Matteoli, M., and De Camilli, P. (1995). Synaptic vesicle dynamics in living cultured hippocampal neurons visualized with CY3-conjugated antibodies directed against the lumenal domain of synaptotagmin. J. Neurosci. *15*, 4328–4342.

Krueger, S. R., Kolar, A., and Fitzsimonds, R. M. (2003). The presynaptic release apparatus is functional in the absence of dendritic contact and highly mobile within isolated axons. Neuron *40*, 945–957.

Malkinson, G. and Spira, M. E. (2006). Calcium concentration threshold and translocation kinetics of EGFP-DOC2B expressed in cultured Aplysia neurons. Cell Calcium. *39*, 85–93.

Marxen, M., Volknandt, W., and Zimmermann, H. (1999). Endocytic vacuoles formed following a short pulse of $K^{+}$-stimulation contain a plethora of presynaptic membrane proteins. Neuroscience *94*, 985–996.

Matteoli, M., Takei, K., Perin, M. S., Sudhof, T. C., and De Camilli, P. (1992). Exo-endocytotic recycling of synaptic vesicles in developing processes of cultured hippocampal neurons. J. Cell. Biol. *117*, 849–861.

Medeiros, N. A., Burnette, D. T., and Forscher, P. (2006). Myosin II functions in actin-bundle turnover in neuronal growth cones. Nat. Cell. Biol. *8*, 215–226.

Morgenthaler, F. D., Knott, G. W., Floyd Sarria, J. C., Wang, X., Staple, J. K., Catsicas, S., and Hirling, H. (2003). Morphological and molecular heterogeneity in release sites of single neurons. Eur. J. Neurosci. *17*, 1365–1374.

Nakhost, A., Kabir, N., Forscher, P., and Sossin, W. S. (2002). Protein kinase C isoforms are translocated to microtubules in neurons. J. Biol. Chem. *277*, 40633–40639.

Patterson, G. H. and Lippincott-Schwartz, J. (2002). A photoactivatable GFP for selective photolabeling of proteins and cells. Science *297*, 1873–1877.

Ryan, T. A. (1999). Inhibitors of myosin light chain kinase block synaptic vesicle pool mobilization during action potential firing. J. Neurosci. *19*, 1317–1323.

Ryu, J., Liu, L., Wong, T. P., Wu, D. C., Burette, A., Weinberg, R., Wang, Y. T., and Sheng, M. (2006). A critical role for myosin IIb in dendritic spine morphology and synaptic function. Neuron *49*, 175–182.

Sahly, I., Erez, H., Khoutorsky, A., Shapira, E., and Spira, M. E. (2003). Effective expression of the green fluorescent fusion proteins in cultured Aplysia neurons. J. Neurosci. Methods. *126*, 111–117.

Sahly, I., Khoutorsky, A., Erez, H., Prager-Khoutorsky, M., and Spira, M. E. (2006). On-line confocal imaging of the events leading to structural dedifferentiation of an axonal segment into a growth cone after axotomy. J. Comp. Neurol. *494*, 705–720.

Sankaranarayanan, S., De Angelis, D., Rothman, J. E., and Ryan, T. A. (2000). The use of pHluorins for optical measurements of presynaptic activity. Biophys. J. *79*, 2199–2208.

Sankaranarayanan, S., Atluri, P. P., and Ryan, T. A. (2003). Actin has a molecular scaffolding, not propulsive, role in presynaptic function. Nat. Neurosci. *6*, 127–135.

Schacher, S. and Proshansky, E. (1983). Neurite regeneration by Aplysia neurons in dissociated cell culture: Modulation by Aplysia hemolymph and the presence of the initial axonal segment. J. Neurosci. *3*, 2403–2413.

Schacher, S. (1985). Differential synapse formation and neurite outgrowth at two branches of the metacerebral cell of Aplysia in dissociated cell culture. J. Neurosci. *5*, 2028–2034.

Shepherd, G. M. and Harris, K. M. (1998). Three-dimensional structure and, composition of CA3–>CA1 axons in rat hippocampal slices: Implications for presynaptic connectivity and compartmentalization. J. Neurosci. *18*, 8300–8310.

Spira, M. E., Dormann, A., Ashery, U., Gabso, M., Gitler, D., Benbassat, D., Oren, R., and Ziv, N. E. (1996). Use of Aplysia neurons for the study of cellular alterations and the resealing of transected axons *in vitro*. J. Neurosci. Methods *69*, 91–102.

Spira, M. E., Oren, R., Dormann, A., and Gitler, D. (2003). Critical calpain-dependent ultrastructural alterations underlie the transformation of an axonal segment into a growth cone after axotomy of cultured Aplysia neurons. J. Comp. Neurol. *457*, 293–312.

Straight, A. F., Cheung, A., Limouze, J., Chen, I., Westwood, N. J., Sellers, J. R., and Mitchison, T. J. (2003). Dissecting temporal and spatial control of cytokinesis with a myosin II Inhibitor. Science *299*, 1743–1747.

Sudhof, T. C. (2004). The synaptic vesicle cycle. Annu. Rev. Neurosci. *27*, 509–547.

Sun, Y. A. and Poo, M. M. (1987). Evoked release of acetylcholine from the growing embryonic neuron. Proc. Natl. Acad. Sci. USA *84*, 2540–2544.

Umeda, T., Ebihara, T., and Okabe, S. (2005). Simultaneous observation of stably associated presynaptic varicosities and postsynaptic spines: Morphological alterations of CA3-CA1 synapses in hippocampal slice cultures. Mol. Cell. Neurosci. *28*, 264–274.

Urakubo, T., Tominaga-Yoshino, K., and Ogura, A. (2003). Non-synaptic exocytosis enhanced in rat cerebellar granule neurons cultured under survival-promoting conditions. Neurosci. Res. *45*, 429–436.

Waites, C. L., Craig, A. M., and Garner, C. C. (2005). Mechanisms of vertebrate synaptogenesis. Annu. Rev. Neurosci. *28*, 251–274.

Whim, M. D., Niemann, H., and Kaczmarek, L. K. (1997). The secretion of classical and peptide cotransmitters from a single presynaptic neuron involves a synaptobrevin-like molecule. J. Neurosci. *17*, 2338–2347.

Zakharenko, S., Chang, S., O'donoghue, M., and Popov, S. V. (1999). Neurotransmitter secretion along growing nerve processes: Comparison with synaptic vesicle exocytosis. J. Cell. Biol. *144*, 507–518.